Nuclear Instruments and Methods in Physics Research A 701 (2013) 1–6

Contents lists available at SciVerse ScienceDirect

Nuclear Instruments and Methods in Physics Research A

journal homepage: www.elsevier.com/locate/nima

A method for the measurement of elastic scattering angular distribution at HIRFL-RIBLL

Y.Y. Yang [a,b], J.S. Wang [a,*], Q. Wang [a], J.B. Ma [a], M.R. Huang [a], J.L. Han [a], P. Ma [a], S.L. Jin [a,b], Z. Bai [a,b], Q. Hu [a,b], L. Jin [a,b], J.B. Chen [a,b], R. Wada [a], Z.Y. Sun [a], R.F. Chen [a], X.Y. Zhang [a], Z.G. Hu [a], X.H. Yuan [a], X.G. Cao [a,1], Z.G. Xu [a], S.W. Xu [a], C. Zhen [a,2], Z.Q. Chen [a], Z. Chen [a,b], S.Z. Chen [a,b], C.M. Du [a,b], L.M. Duan [a], F. Fu [a], B.X. Gou [a,b], J. Hu [a], J.J. He [a], X.G. Lei [a], S.L. Li [a], Y. Li [a,b], Q.Y. Lin [a,b], L.X. Liu [a,b], F.D. Shi [a], S.W. Tang [a,b], G. Xu [a,b], X. Xu [a,b], L.Y. Zhang [a,b], X.H. Zhang [a], W. Zhang [a,b], M.H. Zhao [a,b], Y.H. Zhang [a], H.S. Xu [a]

[a] Institute of Modern Physics, Chinese Academy of Sciences, Lanzhou 730000, China
[b] Graduate University of Chinese Academy of Sciences, Beijing 100049, China

ARTICLE INFO

Article history:
Received 24 August 2012
Received in revised form
30 October 2012
Accepted 30 October 2012
Available online 7 November 2012

Keywords:
Elastic scattering
Radioactive Ion Beams
Monte Carlo simulation

ABSTRACT

A method is presented for the measurement of differential cross-sections of heavy ion elastic scattering induced by Radioactive Ion Beams (RIBs) on the Radioactive Ion Beam Line in Lanzhou (RIBLL) at the Heavy-Ion Research Facility in Lanzhou (HIRFL). The disadvantages of broad beam profiles and limited intensities of the RIBs were overcome using large area detectors, two Parallel-Plate Avalanche Counters (PPACs), two double-sided silicon strip detector (DSSD) telescopes, incorporated with Monte Carlo simulations. The PPACs were used to determine the direction and position of the beam particles. The DSSD telescopes were used to measure scattered particles. Small corrections for the misalignment of detectors and the data normalization were made by assuming the pure Rutherford scattering at very forward angles. The method is suitable for the measurement of the cross-sections on heavy targets at low and intermediate energies, and it has been successfully applied to measure the angular distribution of elastic scattering of ^{7}Be on Pb target at $E_{lab} = 17.9$ MeV/u.

1. Introduction

In recent years, with the development of RIB facilities, a large number of weakly bound nuclei are produced and have been extensively studied. For more than one hundred years after the Rutherford scattering experiment [1], elastic scattering has been used to investigate the properties of nuclei. The nuclear structures of exotic nuclei, such as those with weakly bound nucleon(s), may be reflected on the nuclear reaction mechanisms [2]. Elastic scattering may provide an ideal tool to study the size and shapes of exotic nuclei by comparing similarities and differences between reactions involving weakly bound and stable nuclei [3].

For a scattering experiment, the accurate determination of the scattering angle with the precise direction and position measurement of the incident particles is very crucial. A typical scattering experimental setup requires a target to produce the scattered particles, a series of collimators to collimate incident particles on the target, and position-sensitive detector arrays to determine the direction and position of scattered particles [4]. Silicon strip detectors have been widely used to measure energy and position due to their high energy and spatial resolution. Some of axially symmetric silicon detectors, such as Louvain–Edinburgh Detector Array (LEDA) [5] and Compact Disk double sided silicon strip detector array (CD) [6], are used for the elastic scattering experiments. Such experimental setup has the advantage that the scattering angles are determined by hit annular strips directly if the beam spot and emittance are small enough and the detectors misalignment corrections and normalization are considered. However, it is not suitable in the Radioactive Ion Beam Line in Lanzhou (RIBLL) [7,8] because the beam emittances is large. The designed acceptance of the RIBLL is 50 mm mrad in both X and Y directions. The actual emittances of the secondary beam, in this experimental, is about 31 mm mrad and 41 mm mrad in X and Y directions, respectively, at the secondary target position.

RIBLL has been constructed at the Heavy Ion Research Facility of Lanzhou (HIRFL) [9] and it is in operation since 1998. RIBLL, consisting of four dipoles and sixteen quadrupoles, is designed as a double-achromatic anti-symmetry separator and has three focal points (F0, F2 and F4) and two focal planes (F1 and F3). RIBLL is a

* Corresponding author.
E-mail address: jswang@impcas.ac.cn (J.S. Wang).
[1] Now at Shanghai Institute of Applied Physics, Chinese Academy of Sciences, Shanghai 201800, China.
[2] Now at Institute of Modern Physics, Fudan University, Shanghai 200433, China.

0168-9002/$ - see front matter © 2012 Elsevier B.V. All rights reserved.
http://dx.doi.org/10.1016/j.nima.2012.10.088

Projectile Fragmentation (PF) type facility with a large momentum acceptance and solid angle. Details of the features of design and performance can be found in Refs. [7,8]. The PF method is suitable for providing the RIBs near drip-line with a very short lifetime. However, it has the disadvantage that the beams have a broad distribution in coordinate spaces. Therefore, it is rather difficult to achieve high statistics with enough accuracy using small collimators to provide a well-defined beam for the measurement of elastic scattering cross-sections. In this paper, the experimental method for the measurement of elastic scattering angular distribution was presented in which the disadvantages of the beam qualities were overcome.

2. Measurement

2.1. Production of the secondary beam

The elastic scattering angular distribution of ^{7}Be on a natural Pb target was measured at $E_{lab} = 17.9$ MeV/u. The radioactive nuclear beams of ^{7} Be, together with the contaminants of ^{9}C, ^{8}B and ^{6}Li ions, were produced by the fragmentation of a 54.2 MeV/u ^{12}C primary beam bombarding a 2615 μm thick Be target located at the first focal point (F0) of RIBLL. A 500 μm thick Al plate located at the first focal plane (F1) was used to degrade energy and improve the purity of the selected secondary beam. A 440 μm thick Al plate located at the second focal point (F2), was used to adjust the energy of the beam. The typical intensity of the ^{7}Be secondary beam was 5×10^{3} particles per second with a primary beam intensity of 300 enA. The secondary beams were identified by combining the measured time of flight (TOF) and magnetic rigidity ($B\rho$) value. The TOF was measured using two 50 μm thick plastic scintillation detectors installed at the second (F2) and at the third focal point (F4) with a flight path of 17 m. The $B\rho$ value was determined from the magnetic setting of the third and forth dipole magnets of RIBLL [7,8]. In this measurement, the two dipole magnets were set at the same value.

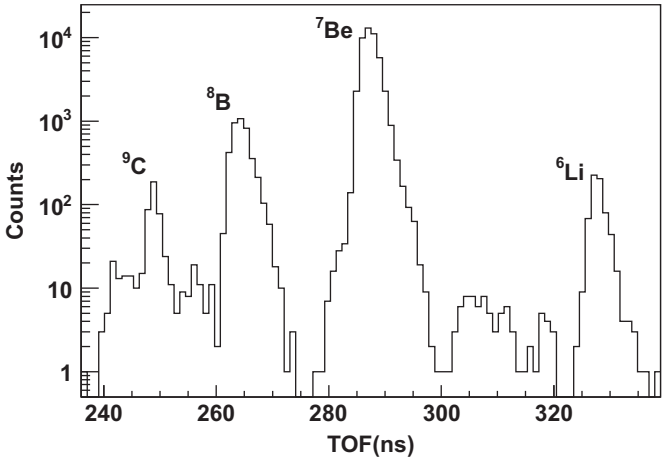

Fig. 1. Time of flight (TOF) spectrum of secondary beams obtained with the two plastic detectors.

In Fig. 1 the typical TOF spectrum is shown. The typical counting rates in the plastic detectors were 4×10^{4} (F2) and 1×10^{4} (F4) particles per second. The contaminants, mainly ^{9}C, ^{8}B and ^{6}Li, can be eliminated in the offline data analysis by applying cuts on the TOF spectrum. The purity of the ^{7}Be secondary beam was about 80%. The beam spot on target had a diameter of 30 mm and a non-uniform distribution in this measurement. The typical beam profiles obtained by two PPACs are shown in Fig. 2.

2.2. Detector setup

The schematic view of the detector setup is shown in Fig. 3. In order to overcome the disadvantages of the large beam spot and low intensity, it is important to measure the position and direction of the beam event by event. For this purpose, two position-sensitive Parallel-Plate Avalanche Counters (PPACs) are used. PPACs have many advantages, such as good position resolution, large sensitive area, almost no disturbance of the incident particles and to be fabricated easily, therefore they are widely used in nuclear reaction experiments [10–12]. Each PPAC consists of two anodes and one cathode. All the electrode planes are kept in parallel to ensure a uniform electric field. The cathode plane in the middle of detector is a 2 μm thick Mylar foil coated with a thin Au-layer on both sides. The two anode planes are located symmetrically on both side of the cathode and consisted of gold-plated tungsten wires. The wires, 50 μm in diameter, are spaced by 1 mm pitch. There are 80 wires in both X and Y directions and therefore the sensitive area is 80×80 mm^{2}. The orientation of the wires on one of the anode planes is perpendicular to the other plane. The signals from the wire electrodes are connected to each other through 4 ns delay lines. The position information is then given by the time difference between the signals from both ends. In Fig. 4 the typical position spectra are shown. The spatial resolution of the PPACs is given by the wire pitch of 1.0 mm. Both the entrance and the exit windows are made by 14 μm Mylar foils and supported by a grid made by a fishing line of 0.5 mm diameter. The PPACs were operated at the voltage of −650 V with a constant gas flow at pressures of 7–

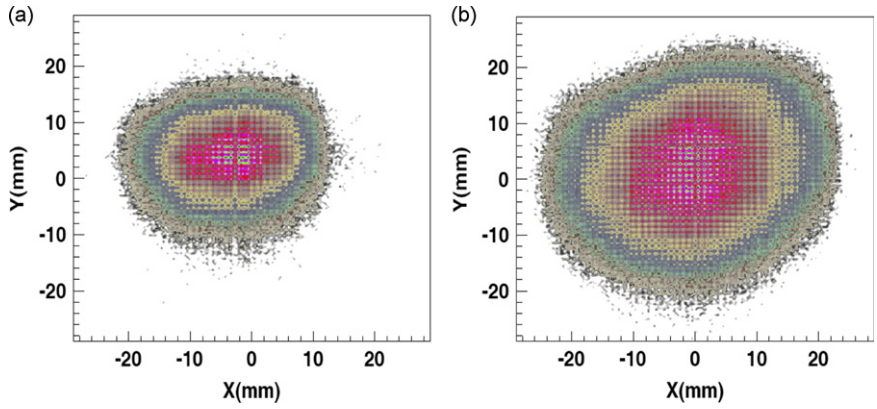

Fig. 2. The typical secondary beam profiles obtained by PPAC1 (a) and PPAC2 (b), respectively.

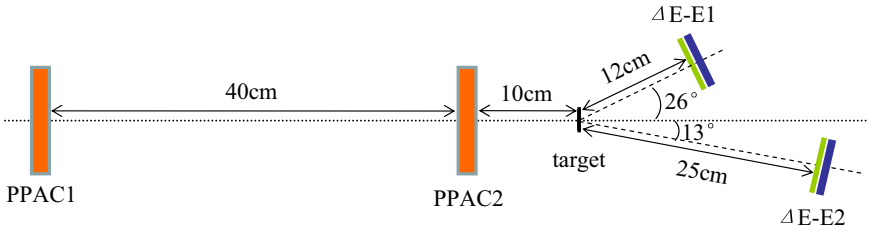

Fig. 3. Schematic view of the detector setup; see text for details.

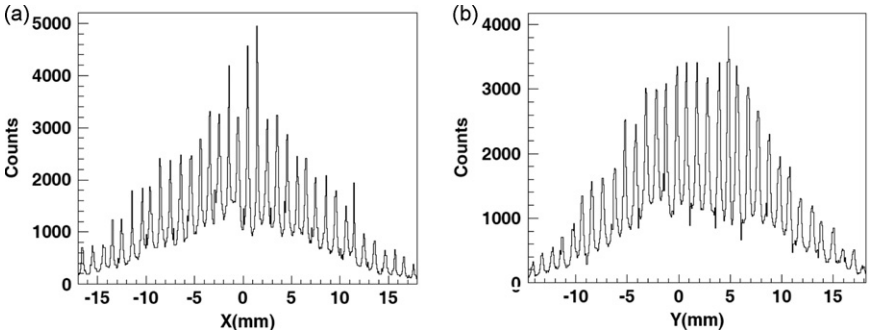

Fig. 4. *X* direction (a) and *Y* direction (b) of secondary beam events recorded in each strip of PPAC2.

9 mbar of isobutane. A control system was used for both PPACs to ensure the stability of the gas pressure and the purity of the gas.

The target used was a self supporting foil of natural Pb with a thickness of 4.2 mg/cm^2. The target had the following isotopic composition: ^{208}Pb 52.3%, ^{207}Pb 22.6%, ^{206}Pb 23.6% and ^{204}Pb 1.48%.

The scattered particles were detected by SiΔE-E telescopes (denoted as ΔE-E1 and ΔE-E2 in Fig. 3). Each telescope consists of one double-sided silicon strip ΔE detector (DSSD) of 150 μm in thickness and 48 × 48 mm^2 in area, and one single silicon detector (SSD) of 1500 μm in thickness and 50 × 50 mm^2 in area. Each DSSD has 48 strips on both sides and the orientations are perpendicular to each other. The DSSDs were used to determine the energy loss and the position of the particles passing through the detector with an accuracy of 1 × 1 mm^2. The SSDs were used to detect the remaining energy. The angular range covered by ΔE-E2 was 4–21° and the ΔE-E1 was 13–38° in the laboratory reference. The angular overlap was made in order to cross-check the differential cross-sections measured by the two telescopes. The energy resolutions (FWHM) of the DSSDs, SSD1 and SSD2 are 0.5–0.9%, 1.2% and 1.3%, respectively, measured by an ^{241}Am α source. ΔE-E telescopes were used to identify the elastic scattering events. Fig. 5 shows a typical two-dimensional particle identification spectrum of ΔE-E2 in the upper panel and one-dimensional energy spectrum of ^{7}Be in the lower panel. The scattered particles ^{7}Be and the contaminants, ^{8}B and ^{6}Li are separated clearly. The energy spectrum of ^{7}Be shows three prominent peaks generated by the elastic scattering from the target (peak1), from a tungsten wire of PPACs (peak2) and from sequential hits of two tungsten wires (peak3), respectively. The yield of ^{7}Be scattering on fishing lines, indicated by the arrow in Fig. 5, is negligible compare to the yield of ^{7}Be scattering on tungsten wires due to the fact than the cross-section of ^{7}Be scattering on tungsten wire is 10^3 times larger than the one on fishing line at the same θ_{lab}. The sigma of peak1 is 1.1 MeV, on account of energy resolution of detector (0.6 MeV) and energy dispersive of secondary beam (0.9 MeV).

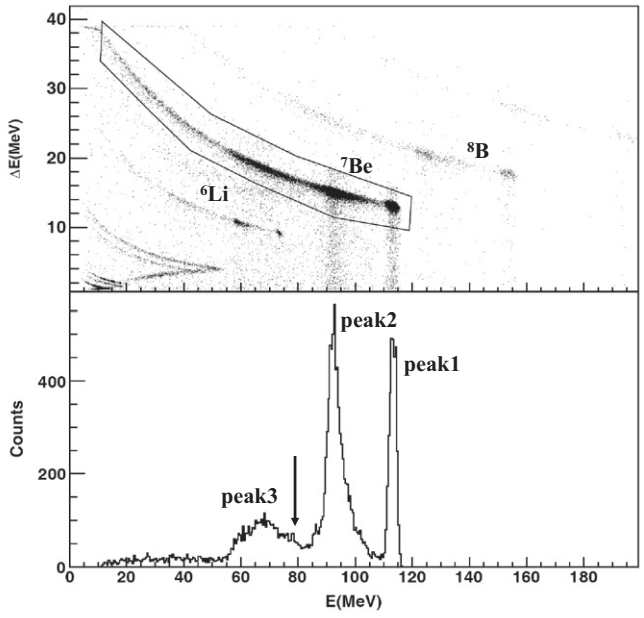

Fig. 5. (a) Two-dimensional particle identification spectrum of ΔE-E2. ΔE is from DSSD2 and E is from the SSD2. (b) One-dimensional energy spectrum. The three peaks generated by the elastic scattering from the target (peak1), from a tungsten wire of PPACs (peak2) and from sequential hits of two tungsten wires (peak3), respectively. The position of the scattering events on fishing line is indicated by the arrow.

2.3. Electronics and data acquisition

The signals of the DSSDs and SSDs were preamplified with modules made by Mesytec [13]. The sensitivity is about 60 mV/MeV for the DSSDs and 10 mV/MeV for the SSDs. The preamplifiers were placed in vacuum chamber and cooled by circulation of cold alcohol at 10 °C. The bias of Si detectors is supplied by a Mesytec MHV-4 power supply. The signals from the preamplifiers were fed to CAEN N568 amplifiers [14]. The timing signals of the PPACs and the plastic scintillators were obtained by Constant Fraction Discriminators (CFD) using the fast preamplifiers outputs. For ^{7}Be ions, the detection efficiencies of PPACs and plastic

detectors were more than 70% and 95%, respectively. Standard CAMAC electronics were used to process the detector signals. The detected particles were recorded on the computer hard disk event by event. Two triggers, TRG1 and TRG2, were provided for the acquisition system

$$\mathrm{TRG1} = (\mathrm{TOF_1} \otimes \mathrm{TOF_2}) \otimes (\mathrm{SSD1} \oplus \mathrm{SSD2}) \otimes (\mathrm{PPAC1} \otimes \mathrm{PPAC2}) \quad (1)$$

$$\mathrm{TRG2} = (\mathrm{TOF_1} \otimes \mathrm{TOF_2}) \otimes (\mathrm{PPAC1} \otimes \mathrm{PPAC2})/1000 \quad (2)$$

where $\mathrm{TOF_1}$ and $\mathrm{TOF_2}$ were from the signals of the plastic scintillation detectors, TRG1 was the trigger of elastic scattering events and TRG2 was that of the beam distribution. An Ortec rate divider (RD2000) [15] was used to reduce the high counting rate of TRG2. The average rates of TRG1 and TRG2 were less than 1 and 7 counts per second, respectively.

3. Data reduction method

The scattering angle (θ), as shown in Fig. 6, was calculated as follows. For an incident particle, a three-dimensional vector AB and the target hit position (x_C, y_C, z_C) were determined by the PPAC1 hit position (x_A, y_A, z_A) and the PPAC2 hit position(x_B, y_B, z_B). The outgoing track was determined by the target hit position and the hit position on DSSD (x_D, y_D, z_D). Scattering angles were calculated event by event using this information on the positions. Fig. 7 shows the histogram of elastic scattering events of ^{7}Be as a function of θ_{lab}, obtained by the ΔE-E2. In order to evaluate the absolute differential cross-sections, a Monte Carlo simulation was used. Assuming the pure Rutherford scattering at all angles, combined with the actual geometry of detector setup and the beam position and direction on PPACs, measured from TRG2, one can obtain the Rutherford scattering yield $N(\theta)_{Ruth}$ at a given θ. After small corrections for misalignment of detectors, described later, the ratio between the experimental and the Rutherford elastic scattering differential cross-sections is obtained by

$$\frac{\frac{d\sigma(\theta)_{exp}}{d\Omega}}{\frac{d\sigma(\theta)_{Ruth}}{d\Omega}} = C \times \frac{N(\theta)_{exp}}{N(\theta)_{Ruth}} \quad (3)$$

where C is a normalization constant, $N(\theta)_{exp}$ and $N(\theta)_{Ruth}$ are the yields at a given angle from the experiment and the simulation, respectively. The normalization constant is a global normalization factor and is determined by imposing that the ^{7}Be elastic scattering cross-sections is the pure Rutherford scattering at very forward angles. This method for obtaining the elastic scattering cross-sections are free from the uncertainties of the calculation of the solid angles, the counts of the total number of beam particles and the target thickness.

The main source of systematic errors in the detector setup comes from possible uncertainties in the position measurement of ΔE-E arrays and PPACs. In actual detector setup, the position determination was made within an uncertainty of 3 mm. Since differential cross–section is very sensitive to the scattered angle, a small angular deviation may result in a significant error in the measurement of the angular distribution. In this experiment, small corrections on the detectors misalignment were required as some other experiments did [2,4,16]. The corrections were made by imposing the pure Rutherford scattering at very forward angles. Monte Carlo simulations from Rutherford scattering were performed to examine the angular distribution of cross-sections as a function of corrections in X -direction, Y -direction, Z-direction and the angle (denoted as angle) between z-axis and the direction normal to the plane of each DSSD, respectively. Some of the simulations for DSSD2 are shown in Fig. 8. In the figure, the ratio of counts with correction (N_e) to those without correction (N_i), N_e/N_i, is plotted as a function of θ_{lab} with -2 mm in X, -2 mm in Y, -5 mm in Z and -1° in angle, respectively. As shown in the figure, the angular distribution is very sensitive to the correction in X -direction, whereas the effects are very small in the Y -direction, Z-direction and angle. Therefore, the detectors misalignment corrections were only made in the X -directions.

The correction of DSSD2 was done by minimizing χ_2^2 in the following formula:

$$\chi_2^2 = \sum_{\theta} \frac{(R(\theta) - \overline{R})^2}{R(\theta)^2} \quad (4)$$

where θ is the corrected scattering angle, $R(\theta)$ is the ratio of experimental to Rutherford elastic scattering cross-sections at a given θ. $\overline{R}$ is the average value of all the points in the angle range between 4° and 12°. The calculations were done in 0.1 mm step

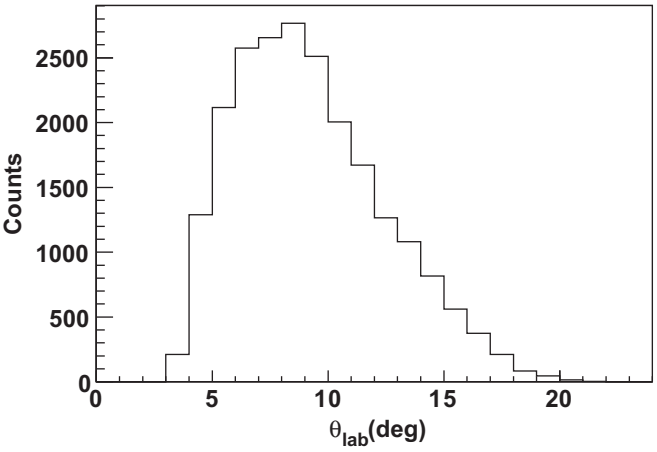

Fig. 7. The histogram of elastic scattering events of ^{7}Be, obtained by the ΔE-E2.

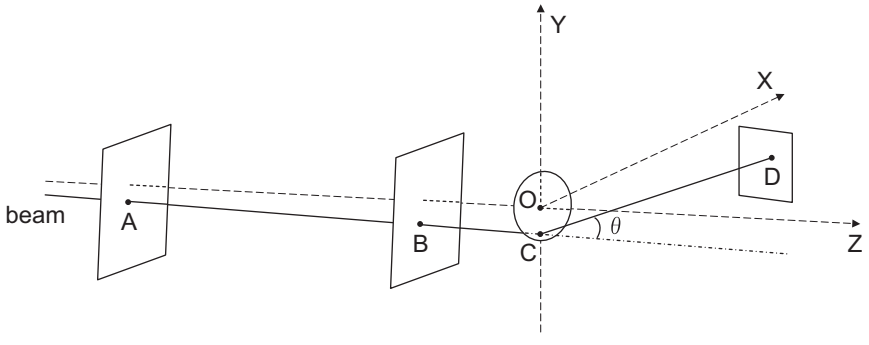

Fig. 6. Diagram of the calculation.

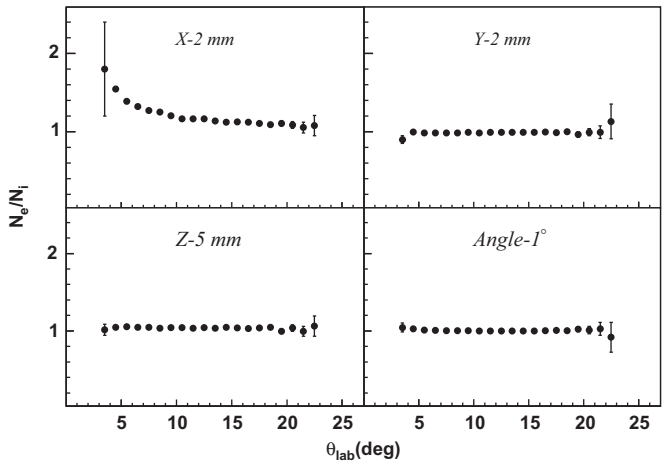

Fig. 8. Some of results of Monte Carlo.

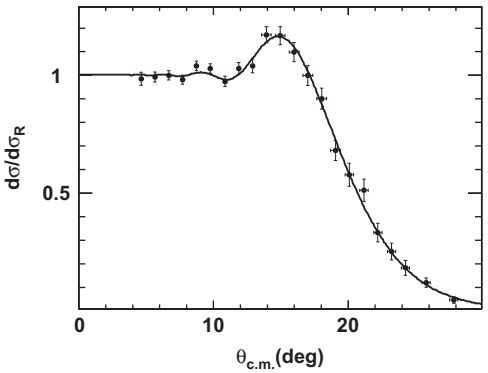

Fig. 9. Ratios of ^{7}Be elastic scattering on Pb target to the Rutherford cross-sections. The experimental data (solid circles) are compared with an optical model calculation (solid line). The error bars in $\theta_{c.m.}$ are smaller that the size of the markers at the angles below 13°.

from 0 mm to +3 mm and the correction of the DSSD2 position in X direction is +2.1 mm with the minimized χ_2^2.

After the correction of DSSD2, the misalignment in DSSD1 was corrected in a different way since the smallest angle is larger than the angles for pure Rutherford scattering. Using the overlapped angles of DSSD1 and DSSD2, which is 13–21°, the correction was performed to minimize the χ_1^2 in the following formula:

$$\chi_1^2 = \sum_{\theta} \frac{(R_S(\theta) - R_L(\theta))^2}{R_L(\theta)^2} \tag{5}$$

where θ is the corrected scattering angle of DSSD1, $R_S(\theta)$ is the ratio of experimental to Rutherford elastic scattering cross-sections at θ in DSSD2 and $R_L(\theta)$ is the ratio at the same angle θ in DSSD1. χ_1^2 were calculated in 0.1 mm step from 0 mm to +3 mm in X -direction of DSSD1. The correction value is +2.4 mm.

4. Results and discussions

The ratio of elastic differential cros-section to the Rutherford cross-section, $d\sigma/d\sigma_{Ruth}$, as a function of center-of-mass angle, θ_{cm}, is shown in Fig. 9. The isotope ^{7}Be has a low-lying bound state at 0.43 MeV that was not identified in this experiment and therefore inelastic yields are included in the data. The error bars of cross-sections in the figure are from statistic only. A systematic error of about 10% should be considered, on account of the scattering events on the windows of PPACs and energy dispersion of secondary beam. The uncertainties of $\theta_{c.m.}$ was calculated, on account of the uncertainties in the positions and spatial resolutions of detectors. The experimental data exhibit a typical elastic scattering behavior. At angles below 12°, the elastic scattering angular distribution shows a small oscillation around 1.0. An obvious interference peak between nuclear and Coulomb potential appears near the grazing angle. After the grazing angle the elastic scattering angular distribution shows an rapid decrease. These data were analyzed in terms of an optical model using the code FRESCO [17]. The angular distribution is well reproduced with a Woods-Saxon potential parameter set: $V_0 = 20.0$ MeV, $R_r = 1.22$ fm, $a_r = 0.80$ fm, $W_0 = 10.2$ MeV, $R_w = 1.36$ fm and $a_w = 0.70$ fm. The measurement and data reduction method described here can be applied to the problems associated with the beams having a broad distribution, non-uniformity and limited intensities. It has been successfully applied to the elastic scattering of ^{7}Be on Pb target at the laboratory energies of 17.9 MeV/u. To minimize the systematic errors, the detectors misalignment corrections and the data normalization were made based on the fact that the differential elastic scattering cross-section is the pure Rutherford scattering at very forward angles. This method has the advantage of avoiding the systematic errors arising from the calculation of the solid angles, total number of beam particles and the target thickness. However, it has a disadvantage that the cross-sections should be measured at small scattering angles in order to use the Rutherford scattering data. For this reason, it is not suitable for the measurement of the cross-sections on light targets and at high energies. Here, it is worth noting the parasitic scattering reactions on the tungsten wires of the PPAC. Recently, it is considered that another type of PPAC [11] with high detection efficiency will be developed and used. The anodes will be made by Au or Al evaporation onto the Mylar foil. In the future, this method will be used to study of elastic scattering angular distribution by the RIBs near the proton or neutron drip-line on heavy targets at low and intermediate energies.

Acknowledgments

We would like to acknowledge the staff of HIRFL for the operation of the cyclotron and friendly collaboration. We are grateful to Dr. D.Y. Pang for informative discussions and Dr. Y.W. Lui for a critical reading of the manuscript. This work is financially supported by the National Natural Science Foundation of China (11005127, 11075190, 10905076), the Directed Program of Innovation Project of Chinese Academy Sciences (Grant no. KJCX2-YW-N44) and the National Basic Research Program of China (973 program, New physics and technology at the limits of nuclear stability)

References

[1] E. Rutherford, Philosophical Magazine 21 (1911) 669.
[2] A. Di Pietro, et al., Physical Review Letters 105 (2010) 022701.
[3] N. Keeley, et al., Physical Review C 77 (2008) 057601.
[4] J. Rahighi, et al., Nuclear Instruments and Methods in Physics Research Section A 578 (2007) 185.
[5] T. Davinson, et al., Nuclear Instruments and Methods in Physics Research Section A 454 (2003) 350.
[6] A.N. Ostrowski, et al., Nuclear Instruments and Methods in Physics Research Section A 480 (2002) 448.
[7] Z. Sun, et al., Chinese Physics Letters 15 (1998) 790.
[8] Z. Sun, et al., Nuclear Instruments and Methods in Physics Research Section A 503 (2003) 496.
[9] J.W. Xia, et al., Nuclear Instruments and Methods in Physics Research Section A 488 (2002) 11.
[10] J. Cub, et al., Nuclear Instruments and Methods in Physics Research Section A 453 (2000) 522.

[11] H. Kumagai, et al., Nuclear Instruments and Methods in Physics Research Section A 470 (2001) 562.
[12] H. Hua, et al., Nuclear Instruments and Methods in Physics Research Section A 481 (2002) 160.
[13] Mesytec GmbH & Co. ⟨http://www.mesytec.com/⟩.
[14] Costruzioni Apparecchiature Elettroniche Nucleari S.p.A. ⟨http://www.caen.it/⟩.
[15] Ortec Products Group ⟨http://www.ortec-online.com/⟩.
[16] L. Acosta, et al., Physical Review C 84 (2011) 044604.
[17] I.J. Thompson, Computer Physics Reports 7 (1988) 167.